Acta Crystallographica Section B
Structural Science
ISSN 0108-7681

Experimental charge density in the transition metal complex $Mn_2(CO)_{10}$: a comparative study

Louis J. Farrugia,[a]* Paul R. Mallinson[a] and Brian Stewart[b]

[a]Department of Chemistry, University of Glasgow, Glasgow G12 8QQ, Scotland, and [b]Department of Chemisty and Chemical Engineering, University of Paisley, Paisley PA1 2BE, Scotland

Correspondence e-mail: louis@chem.gla.ac.uk

Received 18 October 2002
Accepted 8 January 2003

An accurate experimental charge density study at 100 K of $Mn_2(CO)_{10}$ [bis(pentacarbonylmanganese)(Mn—Mn)] has been undertaken. A comparison with previously reported structural determinations reveals no evidence for significant Mn—Mn bond lengthening between 100 and 296 K. The nature of the metal–metal and metal–ligand atom interactions has been studied by topological analysis using the Atoms in Molecules (AIM) approach of Bader [(1990), *Atoms in Molecules: a Quantum Theory*.Oxford: Clarendon Press]. An analysis of the density $\rho(\mathbf{r})$, the Laplacian of the density $\nabla^2\rho(\mathbf{r}_b)$ and the total energy densities $H(\mathbf{r}_b)$ at the bond critical points is used to classify all the chemical bonds as covalent in nature. The results are compared qualitatively and quantitatively with previous charge density studies on this molecule and DFT calculations at the 6-311+G* B3LYP level. The topological properties of the theoretical and experimental densities are in close agreement.

1. Introduction

The nature of metal–metal interactions in low-valent transition metal cluster compounds has been of great interest ever since it was shown (Powell & Ewens, 1939) that the Fe–Fe separation in $Fe_2(CO)_9$ was short enough to constitute a metal–metal bond. The 18-electron or Effective Atom Number (EAN) rule, taught in most undergraduate courses, is often used to infer the presence or otherwise of a direct metal–metal interaction. While this rule is satisfactory in rationalizing the short metal–metal distances often found in these compounds, the situation is much less clear when bridging ligands are present. A classic example of such a controversy concerns $Co_2(CO)_8$, which was shown by theory (Low *et al.*, 1991) and experiment (Leung & Coppens, 1983) to have little or no direct Co—Co bonding, despite the diamagnetic nature of the compound and the prediction of a Co—Co bond from the EAN rule and from earlier theoretical studies (Freund & Hohneicher, 1979; Freund *et al.*, 1980).

The study of the experimental charge density (Coppens, 1997; Tsirelson & Ozerov, 1996; Coppens, 1998; Koritsanszky & Coppens, 2001) offers the possibility of confirming or otherwise the presence of metal–metal and metal–ligand interactions and providing insight into the nature of these interactions. In the past, such studies have been very demanding, requiring many weeks or even months of data acquisition. However, the advent of diffractometers equipped with CCD area detectors has greatly reduced data collection times and has the potential to make charge density studies much more routine. The suitability of CCD detectors with

Table 1
Experimental table.

Chemical formula	$C_{10}Mn_2O_{10}$
Compound color	Orange–yellow
M_r	389.98
Cell setting, space group	Monoclinic, *I*2/*a*
a, *b*, *c* (Å)	14.1257 (2), 6.8799 (1), 14.3121 (3)
β (°)	105.078 (1)
V (Å^3)	1343.01 (4)
Z	4
D_x (Mg m^{-3})	1.929
F(000)	760
Radiation type	Mo $K\alpha$
μ(Mo $K\alpha$) (mm$^{-1)}$	1.930
Crystal size (mm)	0.45 × 0.45 × 0.4
Transmission coefficients (range)	0.417–0.636
θ range (°)	3.31–50.06
Sin θ_{max}/λ	1.079
Temperature (K)	100 (2)
No. of data used for merging	179 392
No. of unique data	7052
Absorption correction	Multi-scan
T_{min}	0.417
T_{max}	0.636
R_{int}	0.0350
R_σ	0.0123
Spherical atom refinement	
No. of data in refinement	7052
No. of refined parameters	101
Final R [$I > 2\sigma(I)$] (all data)	0.0214 (0.0232)
R_w^2 [$I > 2\sigma(I)$] (all data)	0.0608 (0.0616)
Goodness-of-fit S	1.107
Largest features in residual density map (e Å^{-3})	0.619(max) −0.812(min) 0.070(r.m.s.)
Max shift/e.s.d. in last cycle	0.001
Multipole refinement	
No. of data in refinement	6532
No. of refined parameters	296
Final R [$I > 3\sigma(I)$] (all data)	0.0135 (0.0168)
Rw [$I > 3\sigma(I)$]	0.0157
Goodness-of-fit S	2.161
Largest features in residual density map (e Å^{-3})	0.274(max) −0.200(min) 0.044(r.m.s.)
Max shift/e.s.d. in last cycle	0.0036

$R = \sum(|F_o| - |F_c|)/\sum(F_o)$; $Rw = \{\sum[w(F_o - F^c)^2]/\sum[w(F_o)^2]\}^{1/2}$; $R_w^2 = \{\sum[w(F_o^2 - F_c^2)^2]/\sum[w(F_o^2)^2]\}^{1/2}$; $R_\sigma = [\sigma(F_o^2)]/\sum[F_o^2]$; $R_{int} = \sum\{n/(n-1)\}^{1/2}|F_o^2 - F_o^2(mean)|/\sum F_o^2$ (summation is carried out only where more than one symmetry equivalent is averaged).

sealed-tube X-ray sources for accurate electron-density studies has been assessed by a number of authors (Martin & Pinkerton, 1998; Macchi *et al.*, 1998*a*; Macchi, Proserpio, Sironi, Soave & Destro, 1998). The consensus indicates that the data quality is at least as good as from carefully calibrated serial diffractometers, but with an enormous speed advantage. For example, in a recent study on the mineral α-spodumene (Kuntzinger *et al.*, 1999) the relative merits of the Bruker SMART and Nonius KappaCCD diffractometers were compared. It was concluded that both machines gave excellent quality data suitable for charge density work, although the experimental errors appeared to be treated differently by the instrumental software.

Increasingly, the Atoms in Molecules (AIM) approach (Bader, 1990; Popelier, 2000) is being used in the analysis of *experimental* electron density. The method has the great advantage of avoiding the difficult choice of a suitable promolecule and has been adopted in the study of several metal carbonyl or organometallic compounds (Macchi *et al.*, 1998*a*, 1999, 2001; Macchi, Proserpio, Sironi, Soave & Destro, 1998; Scherer *et al.*, 1998; Abramov *et al.*, 1998). An example is the archetypal molecule $Mn_2(CO)_{10}$ (1), which contains an unsupported Mn—Mn bond. The charge density in (1) was originally studied by Martin *et al.* (1982) (hereafter MRM) using deformation density methodology. Little evidence for charge build-up between the Mn atoms was found. Subsequently, Holladay *et al.* (1983) undertook a multipole refinement using this data and determined the *d*-orbital populations. More recently, the charge density in (1) has been re-examined by Bianchi *et al.* (2000) (hereafter BGM) using the AIM approach on newly measured data. A (3,−1) bond critical point (b.c.p.) in $\rho(\mathbf{r})$ at the midpoint of the Mn—Mn vector was observed, but with a very low density and with a small positive value of the Laplacian $\nabla^2\rho(\mathbf{r}_b)$. This result was in reasonable agreement with the theoretical values of MacDougall (1989) and Bo *et al.* (1993) as regards the density, but an opposite sign was predicted for the Laplacian. No critical points corresponding to 1,3 Mn···C interactions between the Mn atom and the carbonyl groups of the other $Mn(CO)_5$ fragment were found in any of these studies. This is in contradiction to some earlier theoretical studies (Brown *et al.*, 1971; Veillard & Rohmer, 1992) which predicted such interactions. On the basis of the magnitudes $\rho(\mathbf{r})$ and $\nabla^2\rho(\mathbf{r}_b)$, BGM interpreted their results in terms of a metallic bond and dative bonds for the Mn—Mn and Mn—C interactions, respectively, related to the ionic 'closed-shell' interaction, as defined by Bader (1990). On the other hand, Macchi & Sironi (2003), in a recent review of charge density studies on transition metal carbonyl compounds, have argued that these bonds should be considered as covalent.

While several comparative charge density studies on organic molecules have been undertaken to investigate the reproducibility of the experimental topology [the best known being the oxalic acid project (Coppens, 1984; Krijn *et al.*, 1988; Zobel *et al.*, 1992; Martin & Pinkerton, 1998)], there have been fewer such studies on transition metal organometallic or coordination complexes. Charge density analyses on the orthorhombic (Bianchi *et al.*, 2001*a*) and triclinic (Bianchi *et al.*, 2001*b*) modifications of $Co_2(CO)_6(\mu\text{-}CO)(\mu\text{-}C_4O_2H_2)$ have been reported. Despite very similar geometries in the two phases, there was only qualitative agreement between the values of $\rho(\mathbf{r}_b)$ and $\nabla^2\rho(\mathbf{r}_b)$ at the b.c.p.'s. Bytheway *et al.* (2001) have shown the reproducibility of topological parameters in the two independent molecules of Cu(glygly)-$(H_2O)_2\cdot H_2O$. Comparative studies are particularly important in view of the well known and recently demonstrated non-uniqueness of the least-squares method in multipole refinement (Pérès *et al.*, 1999) and limited flexibility of the radial functions of the multipole model (Figgis *et al.*, 1993; Iversen *et al.*, 1997; Volkov *et al.*, 2001; Volkov & Coppens, 2001). We herein report our charge density study on $Mn_2(CO)_{10}$ (1), which was under way when the study by BGM was published.

The work reported here is based on data measured with a CCD detector and a laboratory X-ray source, while the previous studies were based on data collected with a scintillation detector. It serves as a comparative study to ascertain the reproducibility and reliablity of multipole refinements on transition metal compounds.

2. Experimental procedures

2.1. Data collection, processing and spherical atom refinement

Compound (1) was obtained from a commercial source. It was resublimed and allowed to evaporate to give a virtually spherical crystal. This was sealed inside a 1 mm Lindeman tube and attached to the tube wall using silicone grease. Details of data collection and refinement procedures are given in Table 1. The crystal sample was cooled from ambient temperature to 100 K over a period of 1 h, using an Oxford Instruments Series 7 Cryostream low-temperature device. The temperature was stable to $\pm$ 0.2 K and is considered accurate to $\pm$0.5 K. Data were collected on a Nonius KappaCCD diffractometer, running under *COLLECT* software (Nonius, 1998). The *COLLECT* (Nonius, 1998) software calculates a strategy to optimize the goniometer and detector angular positions during data acquisition. A total of 4038 image frames were obtained from 93 oscillation runs, with seven different sets of exposure times. The exposure times used were 2, 10, 26, 40, 50, 159 and 180 s per image, with θ_{max} = 31, 30, 36, 45, 30, 55 and 56°, respectively, totalling 102.8 h of exposure time. Oscillation angles of 1.7 or 2.0° were used, with the oscillation axis being either the diffractometer ω or φ axis. Batch scaling factors for each oscillation run within each of the seven sets showed no consistent variation over time, indicating no significant sample decay. The high-angle sets utilized the longer exposure times to improve the measurement statistics, while the shorter exposure times were used to accurately record the intense low-order data, avoiding pixel overflow or integration failure. The scan sets with small θ offsets were measured first in the data collection strategy, in order to alleviate problems with ice rings which gradually build up during data collection. The high-angle images showed no evidence of contamination from ice rings. The unit-cell dimensions used for refinement purposes were determined by post-refinement of the setting angles of a significant portion of data set 4 (12 609 reflections with $3 < \theta < 45°$) using the *SCALEPACK* program (Otwinowski & Minor, 1997). The cell errors obtained from this least-squares procedure are undoubtedly serious underestimates (Herbstein, 2000), but are used here in the absence of better estimates. The cell determination procedures are not in the public domain, as they are components of commercial software (Otwinowski & Minor, 1997), but a study of Paciorek *et al.* (1999) suggests that less accurate results are to be expected from oscillation methods than for standard scintillation counter diffractometers. The accuracy depends critically on the frame widths and data spanning. In line with these observations, we find that the unit cells obtained from our seven sets of exposure times vary by a much higher percentage than the extremely low s.u.'s would suggest – the cell volumes range from 1340.1 to 1344.5 Å^3. The rationale for choosing the unit cell derived from data set 4 was that the resolution was reasonably high (θ_{max} = 45°), but not high enough to cause integration software problems with $K_{\alpha1\,-\,\alpha2}$ splitting. The unit-cell volume for (1), determined at 103 K at the SRS Daresbury with λ = 0.4901 Å (Farrugia & Mallinson, 2002), was virtually identical to that reported here. While the literature discussions on unit-cell measurements tend to focus on precision rather than accuracy (Herbstein, 2000), we note that *accurate* rather than *precise* unit cells are required for a meaningful comparison between studies from different laboratories. The current reliance on commercial 'black box' data processing software for unit-cell determination and frame integration is not entirely satisfactory for accurate studies.

The frame images were integrated using *DENZO(SMN)* (Otwinowski & Minor, 1997), with spot elongation for the high-angle data, in order to (at least partially) account for the $K_{\alpha1\,-\,\alpha2}$ splitting, which becomes quite significant at $\theta \simeq 50°$. In our experience the neighborhood profiling used in *DENZO(SMN)* appears to cope quite well with this problem. Graafsma *et al.* (1997) have also reported the successful use of *DENZO* for integrating synchrotron data used in a charge density study. The resultant raw intensity files from *DENZO(SMN)* were processed using a locally modified version of *DENZOX* (Blessing, 1997*a*), which calculates direction cosines for the absorption correction, as well as applying rejection criteria on the basis of bad χ^2 of profile-fit and ignoring partial reflections at the starting or final frame of a scan set. A total of 179 392 intensity measurements, excluding space-group extinctions, were harvested from the image files. A semi-empirical absorption correction (Blessing, 1995) with a theta dependency was applied, to account for the absorption of the spherical crystal and remove any anisotropy due to the mounting medium. The resulting data were sorted and merged using *SORTAV* (Blessing, 1997*b*), giving 7052 independent data with a mean redundancy of 25.0 and to a resolution of $\sin(\theta_{max})/\lambda$ = 1.0788 (θ_{max} = 50° for Mo $K\alpha$ radiation). Four low-angle data are absent, since all measurements of these reflections apparently suffered from complete or partial truncation by the beamstop. The data were integrated and processed using the standard space-group setting of *C*2/*c*, but were transformed to *I*2/*a* for refinement purposes, since this gives a monoclinic β angle much closer to 90°. However, the atomic labeling scheme of BGM was used to facilitate a direct comparison. A spherical atom refinement using *SHELXL*97 (Sheldrick, 1997) was initially undertaken, with full-matrix least-squares on F^2 and using all the unique data with the weighting scheme $w = [\sigma(F_o)^2 + (AP)^2 + BP]^{-1}$, where $P = [F_o^2/3 + 2F_c^2/3]$ and A = 0.0288, B = 0.3769. All atoms were allowed anisotropic thermal motion. An empirical extinction correction parameter x (Sheldrick, 1997) was refined, which gave a final value of 0.0107 (5). Neutral atom scattering factors, coefficients of anomalous dispersion and absorption coefficients were as supplied in *SHELXL*97

(Sheldrick, 1997). Details of this refinement are given in Table 1. Thermal ellipsoid plots were obtained using the program *ORTEP*3 for Windows (Farrugia, 1997). All calculations were carried out using the *WinGX* package (Farrugia, 1999) of crystallographic programs.

2.2. Multipole refinement

The multipole formalism of Hansen & Coppens (1978) as implemented in the *XD* program suite (Koritsanszky *et al.*, 1997) was applied. The version of *XD* as modified by Macchi (Macchi *et al.*, 2001) was used, as this version can utilize relativistic scattering factors and also incorporates a number of important corrections related to the treatment of transition metals. The function minimized in the least-squares procedure was $\Sigma w(|F_o| - k|F_c|)^2$, with only those reflections with $I > 3\sigma(I)$ included in the refinement. The multipole expansion was truncated at the hexadecapole level for the Mn atoms and at the octupole level for C and O atoms. Each pseudoatom was assigned a core and spherical-valence scattering factor derived from the relativistic Dirac–Fock wavefunctions of Su & Coppens (1998) expanded in terms of the single-ζ functions of Bunge *et al.* (1993). The radial fit of these functions was optimized by refinement of the expansion–contraction parameter κ. The valence deformation functions for the C and O atoms used a single-ζ Slater-type radial function multiplied by the density-normalized spherical harmonics. The radial fits were optimized by refinement of their expansion–contraction parameters κ', a single parameter being used for each elemental type. The radial terms used for the Mn atoms were either simple Slater functions (for l = 1, 3) or the relevant order Fourier–Bessel transforms of the Su & Coppens (1998) wavefunctions (for l = 0, 2, 4). It is well established (Coppens, 1985) that the 3*d* transition metals present special problems when refining the deformation density because of the significantly different radial extentions of the 3*d* and 4*s* valence orbitals. In view of these problems, it is common practice to treat the 4*s* density as 'core' density (even though it is patently not so), since the scattering from this density is only significant for $\sin\theta/\lambda < \sim 0.20$ (Martin *et al.*, 1982). In the current data set, only 40 reflections satisfy this criterion and hence have a significant scattering contribution from the 4*s* density. In view of this, it is not surprising that attempts to refine the 4*s* population independently through the l = 0 deformation function (the second monople) were unsuccessful. All such models proved unstable or gave physically unrealistic populations. Models based on the $3d^7$ electron configuration were also initially examined, but these gave significantly worse residuals and some physically unrealistic model parameters, and were not considered further. The final model used was based on the $4s^2 3d^n$ configuration. This ambiguity in the 4*s* population has implications for the definition of the atomic charge discussed below. The rigid-bond criterion of Hirshfeld (1976) was fulfilled for all C—O bonds (mean $\Delta_{A,B}$ = 0.7×10^{-3} Å^2), except for C1—O1 ($\Delta_{A,B} = 1.2 \times 10^{-3}$ Å^2). As we have previously observed for metal–ligand bonds (Smith *et al.*, 1997), the $\Delta_{A,B}$ value for the Mn—C bonds is slightly higher (mean value = 1.5×10^{-3} Å^2) than the Hirshfeld criterion. This discrepancy may reflect some inadequacy in the radial functions used for the Mn atom, incomplete deconvolution of the thermal parameters or a breakdown in the applicability of the Hirshfeld criterion for transition metal/light-atom bonds (Bürgi, 1984).

An isotropic extinction correction (Becker & Coppens, 1974) of Type I with a Gaussian distribution of mosaic spread and mosaic distribution Type I (mosaic spread = 25.21′) was applied, with g' refining to 0.231 (7). Extinction effects are, however, very minor in this crystal, with only 15 reflections having $y < 0.9$. The worst affected reflection was (−4 0 −2), with y = 0.44. A scatterplot of F_{obs} against F_{calc} confirmed this lack of extinction effects, but implied that the weakest reflections were systematically overestimated. This is not apparently due to any $\lambda/2$ contamination (Kirschbaum *et al.*, 1997), since $\langle F_{obs} - F_{calc}\rangle$ for reflections with all indices even is slightly lower than for those reflections with two odd indices. A scatterplot of $F_{obs} - F_{calc}$ against $\sin\theta/\lambda$ showed little discernable trend.

In order to gauge the reproducibility and model dependence of the integrated atomic properties calculated by the *TOPXD* program (Volkov, Gatti *et al.*, 2000), two different multipole models were tested in these calculations. MODEL1 is as described above, while MODEL2 was slightly less flexible. The differences in MODEL2 are:

(i) the scattering factors are computed from Clementi–Roetti wavefunctions rather than the relativistic Dirac–Fock functions and

(ii) a single-ζ Slater-type radial function was used for the Mn atom rather than Hartree–Fock-based functions.

The differences are small and for the monopole-derived charges $q(Pv)$ they are well within the computed errors. The *precision* of numerical integration may be gauged from the value of the atomic Lagrangian $L(\Omega)$, which is proportional to the integrated flux of the gradient vector field of ρ at the interatomic surface and should be equal to zero in the ideal case. In practice, a reasonable absolute value is considered to be $< \sim 1 \times 10^{-3}$ a.u. (Volkov, Gatti *et al.*, 2000). The mean absolute value of $L(\Omega)$ was 1.3×10^{-3} a.u., with the greatest value of 4.6×10^{-3} a.u. for the Mn atom. The overall charge discrepancy (sum of net charges) was 0.03 a.u. for the crystallographically independent $Mn(CO)_5$ unit. This is slightly higher than expected and is probably due to the complexity of the interatomic surfaces, especially of the Mn atom. Nevertheless, it represents only 0.03% of the total electron population. The total integrated atomic volume per cell (MODEL 1) is 1338.4 Å^3, compared with the measured cell volume of 1343.01 (4) Å^3, an error of 0.34%. Several recent studies (Flensburg & Madsen, 2000; Aicken & Popelier, 2000; Volkov, Gatti *et al.*, 2000; Bytheway *et al.*, 2002) suggest a conservative estimate of $\sim \pm 5\%$ for the *accuracy* of the integrated atomic properties, although some properties, *e.g.* electron populations, are much less sensitive to errors than others.

The kinetic energy densities at the b.c.p.'s $G(\mathbf{r})$ given in Table 2 for the experimental densities were estimated using the functional approximation of Abramov (1997)

Table 2
Topological analysis of (3,−1) bond critical points in ρ.

Top line: experimental values from this study; second line: experimental values from BGM study (Bianchi *et al.*, 2000); third, fourth and fifth lines: theoretical values from DFT calculations with BASIS 1, BASIS 2 and BASIS 3, respectively (see text). R_{ij}: length of bond path; d_i d_j: distances of b.c.p. from atoms 1/2, in units of Å. $\rho(\mathbf{r}_b)$ in units of e Å^{-3}; $\nabla^2\rho(\mathbf{r}_b)$, λ_1, λ_2, λ_3 in units of e Å^{-5}; $G(\mathbf{r}_b)$, $V(\mathbf{r}_b)$ and $H(\mathbf{r}_b)$ in units of Hartree Å^{-3}. $G(\mathbf{r}_b)$ estimated by the approximation of Abramov (1997). $R_{\rm para} = \Sigma\,(|P_{\rm exp} - P_{\rm theor}|)/\Sigma|P_{\rm theor}|$. Top line: $R_{\rm para}$ from this study; second line: calculated from BGM study.

Bond	R_{ij}	d_i	$d_2 \times d_j$	$\rho(\mathbf{r}_b)$	$\nabla^2\rho(\mathbf{r}_b)$	λ_1	λ_2	λ_3	ε	$G(\mathbf{r}_b)$	$G(\mathbf{r}_b)/\rho(\mathbf{r}_b)$	$V(\mathbf{r}_b)$	$H(\mathbf{r}_b)$
Mn1—Mn1*A*	2.9078	1.4518	1.4518	0.144 (3)	0.720 (3)	−0.05	−0.04	0.81	0.10	0.07	0.45	−0.08	−0.02
	2.9054	1.4527	1.4527	0.190 (4)	0.815 (8)	−0.197 (3)	−0.197 (3)	1.209 (6)	0.0	0.088	0.466	−0.12	−0.031
	2.9065	1.4533	1.4532	0.200	−0.071	−0.312	−0.304	0.545	0.027	0.057	0.282	−0.118	−0.062
	2.9066	1.4533	1.4533	0.198	−0.046	−0.290	−0.284	0.528	0.021	0.056	0.285	−0.116	−0.060
	2.9060	1.4530	1.4530	0.192	0.124	−0.272	−0.259	0.654	0.050	0.060	0.314	−0.112	−0.052
Mn1—C1	1.8235	0.9262	0.8967	0.952 (6)	12.855 (13)	−4.07	−3.89	20.81	0.05	1.34	1.41	−1.78	−0.44
	1.822	0.932	0.890	1.06 (2)	16.1 (3)	−4.40 (5)	−3.97 (5)	24.5 (3)	0.11	1.64	1.54	−2.15	−0.51
	1.8228	0.9144	0.9084	0.924	13.507	−3.577	−3.548	20.633	0.008	1.315	1.424	−1.685	−0.370
	1.8228	0.9183	0.9046	0.935	12.647	−3.432	−3.399	19.478	0.010	1.71	1.360	−1.658	−0.386
	1.8228	0.9152	0.9076	0.894	13.564	−3.085	−3.044	19.692	0.013	1.298	1.452	−1.646	−0.348
Mn1—C2	1.8675	0.9195	0.9430	0.820 (5)	13.420 (11)	−3.11	−3.05	19.58	0.02	1.20	1.47	−1.47	−0.26
	1.908	0.9248	0.9832	0.66 (2)	14.3 (3)	−2.50 (5)	−1.18 (5)	18.0 (3)	1.12	1.07	1.62	−1.14	−0.07
	1.8642	0.9243	0.9399	0.828	13.227	−3.152	−3.070	19.449	0.026	1.194	1.442	−1.463	−0.268
	1.8641	0.9271	0.9370	0.840	12.319	−3.025	−2.959	18.302	0.022	1.163	1.385	−1.463	−0.301
	1.8615	0.9222	0.9394	0.801	13.196	−2.723	−2.674	18.593	0.018	1.195	1.491	−1.465	−0.271
Mn1—C3	1.8599	0.9131	0.9440	0.804 (5)	14.396 (12)	−2.95	−2.57	19.92	0.15	1.23	1.53	−1.45	−0.22
	1.866	0.935	0.931	0.85 (2)	14.5 (2)	−3.81 (3)	−2.55 (3)	20.9 (2)	0.49	1.29	1.51	−1.56	−0.27
	1.8590	0.9186	0.9403	0.826	13.649	−3.023	−2.878	19.550	0.05	1.219	1.476	−1.483	−0.264
	1.8588	0.9215	0.9373	0.838	12.739	−2.913	−2.753	18.405	0.058	1.188	1.418	−1.484	−0.296
	1.8577	0.9189	0.9388	0.802	13.445	−2.688	−2.508	18.641	0.072	1.211	1.511	−1.481	−0.270
Mn1—C4	1.8633	0.9142	0.9462	0.806 (6)	13.815 (12)	−3.02	−2.73	19.56	0.11	1.21	1.50	−1.44	−0.24
	1.9075	0.9504	0.9571	0.78 (2)	11.8 (2)	−4.37 (3)	−2.89 (3)	19.1 (2)	0.51	1.08	1.39	−1.34	−0.26
	1.8650	0.9255	0.9395	0.828	13.238	−3.160	−3.068	19.466	0.03	1.196	1.445	−1.465	−0.269
	1.8650	0.9284	0.9365	0.839	12.325	−3.034	−2.953	18.313	0.027	1.164	1.387	−1.465	−0.301
	1.8623	0.9234	0.9389	0.800	13.236	−2.740	−2.633	18.609	0.041	1.197	1.496	−1.468	−0.271
Mn1—C5	1.8744	0.9137	0.9541	0.800 (6)	13.993 (11)	−2.83	−2.72	19.54	0.04	1.21	1.51	−1.44	−0.23
	1.880	0.9419	0.9381	0.85 (2)	13.3 (2)	−4.13 (3)	−2.92 (3)	20.3 (2)	0.41	1.23	1.45	−1.54	−0.30
	1.8694	0.9228	0.9466	0.808	13.407	−2.913	−2.864	19.184	0.017	1.185	1.467	−1.432	−0.247
	1.8692	0.9254	0.9438	0.820	12.483	−2.809	−2.752	18.044	0.021	1.155	1.409	−1.437	−0.282
	1.8673	0.9218	0.9455	0.784	13.209	−2.587	−2.514	18.310	0.029	1.181	1.506	−1.437	−0.256
O1—C1	1.1485	0.7672	0.3802	3.108 (15)	24.13 (11)	−31.85	−30.27	86.24	0.05	6.45	2.07	−11.21	−4.76
	1.148	0.742	0.406	3.69 (9)	−45 (5)	−44 (3)	−43 (3)	42 (5)	0.02	5.0	1.4	−13.1	−8.1
	1.1472	0.7466	0.4006	2.923	12.583	−31.446	−31.417	75.446	0.001	5.234	1.790	−9.587	−4.353
	1.1472	0.7659	0.3813	3.129	24.662	−33.501	−33.485	91.648	0.0	6.979	2.230	−12.232	−5.253
	1.1472	0.7653	0.3819	3.138	23.293	−33.582	−33.555	90.429	0.001	6.944	2.213	−12.257	−5.313
O2—C2	1.1421	0.7612	0.3808	3.123 (11)	20.88 (8)	−32.11	−31.51	84.49	0.02	6.34	2.03	−11.22	−4.88
	1.142	0.735	0.407	3.25 (8)	−24 (3)	−36 (2)	−32 (2)	44 (2)	0.12	4.6	1.4	−10.9	−6.3
	1.142	0.7433	0.3987	2.961	14.193	−32.446	−32.289	78.928	0.005	5.431	1.834	−9.868	−4.437
	1.1420	0.7620	0.3800	3.166	26.316	−34.265	−34.150	94.731	0.003	7.157	2.261	−12.472	−5.315
	1.1420	0.7615	0.3805	3.175	24.892	−34.368	−34.277	93.537	0.003	7.121	2.243	−12.500	−5.379
O3—C3	1.1438	0.7625	0.3812	3.106 (12)	21.02 (8)	−31.56	−30.92	83.50	0.02	6.30	2.03	−11.12	−4.83
	1.142	0.706	0.436	3.57 (7)	−44 (2)	−36 (1)	−33 (1)	25 (1)	0.09	4.6	1.3	−12.4	−7.7
	1.1437	0.7445	0.3993	2.948	−32.170	−31.967	77.895	0.006	5.37	1.822	−9.777	−4.407	
	1.1437	0.7633	0.3804	3.154	25.793	−34.066	−33.899	93.758	0.005	7.100	2.251	−12.394	−5.294
	1.1437	0.7628	0.3809	3.163	24.419	−34.174	−33.999	92.592	0.005	7.067	2.234	−12.424	−5.357
O4—C4	1.1435	0.7621	0.3813	3.142 (11)	18.75 (8)	−32.96	−30.91	82.62	0.07	6.29	2.0	−11.28	−4.98
	1.140	0.721	0.419	3.36 (7)	−32 (2)	−34 (1)	−31 (1)	33 (1)	0.10	4.6	1.4	−11.4	−6.8
	1.1433	0.7442	0.3991	2.951	13.858	−32.250	−32.041	78.15	0.007	5.385	1.825	−9.799	−4.415
	1.1433	0.7630	0.3803	3.157	25.976	−34.105	−33.943	94.024	0.005	7.117	2.255	−12.416	−5.299
	1.1433	0.7624	0.3808	3.166	24.581	−34.215	−34.058	92.854	0.005	7.082	2.237	−12.444	−5.362
O5—C5	1.1422	0.7619	0.3802	3.190 (12)	18.30 (8)	−33.47	−32.34	84.11	0.03	6.41	2.01	−11.54	−5.13
	1.139	0.688	0.451	3.87 (7)	−57 (2)	−42 (1)	−39 (1)	24 (1)	0.08	4.9	1.3	−13.7	−8.9
	1.142	0.7434	0.3986	2.960	14.263	−32.440	−32.294	78.996	0.005	5.434	1.836	−9.870	−4.436
	1.1420	0.7621	0.3800	3.166	26.359	−34.260	−34.147	94.766	0.003	7.159	2.261	−12.472	−5.314
	1.1420	0.7615	0.3805	3.175	24.854	−34.369	−34.286	93.510	0.002	7.120	2.242	−12.499	−5.380

Table 2 (continued)

Bond	R_{ij}	d_i	$d_2 \times d_j$	$\rho(\mathbf{r}_b)$	$\nabla^2\rho(\mathbf{r}_b)$	λ_1	λ_2	λ_3	ε	$G(\mathbf{r}_b)$	$G(\mathbf{r}_b)/\rho(\mathbf{r}_b)$	$V(\mathbf{r}_b)$	$H(\mathbf{r}_b)$
$R_{\rm param}$ BASIS 1	0.0008	0.0140	0.0156	0.0559	0.2797	0.0236	0.0317	0.0675	2.6923	0.1523	0.0838	0.1357	0.1165
	0.0064	0.0214	0.0271	0.1788	2.0449	0.2038	0.1345	0.4715	16.0549	0.1171	0.1737	0.2423	0.6881
$R_{\rm param}$ BASIS 2	0.0008	0.0056	0.0057	0.0163	0.1709	0.0500	0.0809	0.0981	2.7943	0.1022	0.0943	0.0839	0.0790
	0.0064	0.0296	0.0388	0.1177	1.7766	0.1462	0.1258	0.5560	16.6686	0.2925	0.2805	0.0835	0.4197
$R_{\rm param}$ BASIS 3	0.0012	0.0042	0.0050	0.0163	0.1296	0.0603	0.0872	0.0855	1.7615	0.0833	0.0663	0.0859	0.0868
	0.0069	0.0308	0.0386	0.1178	1.7528	0.1495	0.1288	0.5483	12.1799	0.2983	0.2588	0.0840	0.4051

$$G(\mathbf{r}) = (3/10)(3\pi^2)^{2/3}\rho(\mathbf{r})^{5/3} + (1/6)\nabla^2\rho(\mathbf{r}),$$

while the corresponding potential energy densities at the b.c.p.'s $V(\mathbf{r})$ were obtained from the local virial relationship (expressed in a.u.), as shown by Bader (1990)

$$V(\mathbf{r}) = (1/4)\nabla^2\rho(\mathbf{r}) - 2G(\mathbf{r}).$$

The above approximation for $G(\mathbf{r})$ holds well for closed-shell interactions, where $\nabla^2\rho(\mathbf{r}) > 0$ (Abramov, 1997), and is a good approximation for all the covalent bonds in (1) (see §2.3).

2.3. Theoretical calculations

SCF (self-consistent field) calculations used the DFT option of the *GAMESS-UK* program suite (Guest *et al.*, 2002). Wavefunction files suitable for direct reading by AIMPAC and other analysis programs were obtained using the 'save aimpac' option. The topological properties were examined with a minimal basis 3–21 G (BASIS 1), a more extensive basis using Alrichs pVDZ parameterization for Mn (BASIS 2) (Schafer *et al.*, 1992) and a basis set employing diffuse functions with Wachters parameterization for Mn (BASIS 3). The B3LYP function (Becke, 1993) was used throughout. The BASIS 3 calculations used a 6-31 + G* basis for C and O and the Wachters basis with additional *f* polarization functions for Mn (Wachters, 1969, 1970). *F* exponents were obtained from Bauschlicher *et al.* (1989). Two additional *s*- and *p*-type diffuse functions were added for Mn with the exponents obtained by logarithmic extrapolation of the Wachters *s* and *p* functions. Wachters and Ahlrichs basis sets were obtained from the Extensible Computational Chemistry Environment Basis Set Database, Version 7/30/02, as developed and distributed by the Molecular Science Computing Facility, Environmental and Molecular Sciences Laboratory.

Single-point calculations at the experimental C_2 geometry of the isolated molecule were performed, with no geometry optimization. Preliminary calculations using the BGM C_2 experimental geometry were also undertaken, but gave very similar results and are not reported further. Atomic properties were obtained from the theoretical densities using a locally modified version of the *AIMPAC* programs (Biegler-König *et al.*, 1982), *AIM*2000 (Biegler-König, 2000) or the *MORPHY*98 program (Popelier, 1998). The integrated charges $q(\Omega)$ and topological properties at the bond critical points are given in Tables 2 and 3, respectively; other properties are deposited as supplementary material.[1] We find only a minor dependency of $q(\Omega)$ on the basis set, in line with the observations of Cioslowski *et al.* (1990). Critical points in the Laplacian function, $L(\mathbf{r}) \equiv -\nabla^2\rho(\mathbf{r})$, in the *i*-VSCC of the Mn atom were searched using the BUBBLE algorithm (Krug & Bader, 1990), for both the theoretical and experimental densities. One of the 12 (3,−1) saddle c.p.'s in the experimental density could not be found automatically in this way and was obtained from its approximated position.

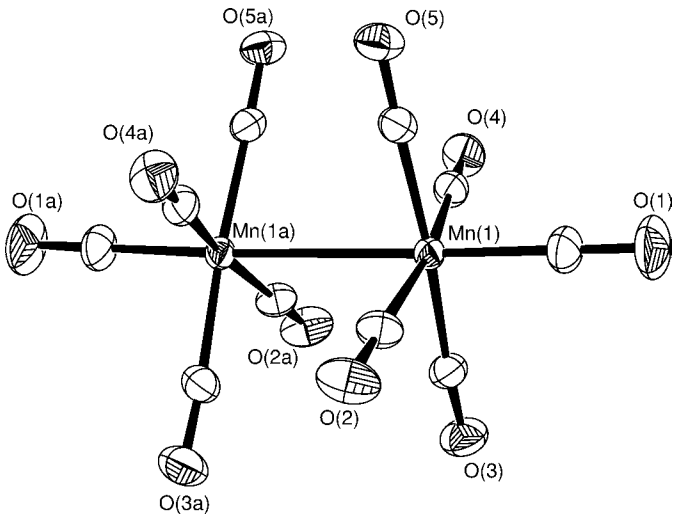

Figure 1
ORTEP (Farrugia, 1997) view of $Mn_2(CO)_{10}$ (1) showing the atomic labelling scheme.

3. Results and discussion

3.1. Description of the structure

An *ORTEP* (Farrugia, 1997) view of (1), showing the atomic labelling scheme, is given in Fig. 1. Compound (1) has been the subject of accurate determinations at 74 K by Martin *et al.* (1982), at 120 K by Bianchi *et al.* (2000) and at ambient temperature by Churchill *et al.* (1981). The important metrical parameters for (1), taken from all these studies, are compared in Table 4 with the parameters determined in this work. The two $Mn(CO)_5$ fragments are related by a crystallographic twofold axis. The well known structural features of (1) are reproduced in our study and merit little further comment. The bond angles are remarkably consistent between data sets, generally agreeing within a few σ, but the Mn—C and C—O distances in our study are on average ∼0.25% larger than the means for the other two low-temperature studies. The most

[1] Supplementary data for this paper are available from the IUCr electronic archives (Reference: BS0019). Services for accessing these data are described at the back of the journal.

Table 3
Atomic charges (a.u.).

[a] This study, experimental density using MODEL 1 refinement; [b] this study, experimental density using MODEL 2 refinement; [c] this study, theoretical DFT density 6-311G*(C,O) *p*VDZ-Ahlrichs(Mn); [d] from integration using intersecting spheres, taken from Martin *et al.* (1982); [e] from κ refinement, taken from Martin *et al.* (1982); [f] taken from Bianchi *et al.* (2000).

Atom	$q(Pv)^a$	$q(Pv)^b$	$q(\Omega)^a$	$q(\Omega)^b$	$q(\Omega)^c$	MRM[d]	MRM[e]	$q(Pv)^f$
Mn1	0.68 (4)	0.74 (4)	1.164	1.084	0.913	−0.16	0.92	−0.2 (3)
O1	0.08 (4)	0.06 (4)	−1.186	−1.159	−1.195	0.05	0.02 (5)	0.16 (5)
O2	0.11 (3)	0.08 (3)	−1.164	−1.183	−1.198	−0.09	−0.55 (4)	0.13 (3)
O3	0.04 (3)	0.01 (4)	−1.220	−1.240	−1.190	−0.01	−0.46 (4)	0.12 (4)
O4	0.07 (3)	0.03 (3)	−1.211	−1.232	−1.193	−0.05	−0.51 (4)	0.15 (3)
O5	0.13 (3)	0.08 (3)	−1.167	−1.188	−1.195	0.02	−0.40 (4)	0.23 (3)
C1	−0.21 (4)	−0.16 (4)	0.991	0.941	1.004	0.01	−0.35 (6)	−0.11 (5)
C2	−0.18 (4)	−0.16 (4)	0.994	1.017	1.007	0.04	0.01 (4)	0.09 (4)
C3	−0.26 (4)	−0.24 (4)	0.915	0.928	1.013	0.06	−0.06 (5)	−0.26 (5)
C4	−0.21 (4)	−0.19 (4)	0.976	1.049	1.006	0.06	0.10 (4)	−0.14 (4)
C5	−0.27 (4)	−0.24 (4)	0.937	1.013	1.015	0.05	−0.08 (5)	−0.16 (4)
Max $\|L(\Omega)\|$	–	–	2.6×10^{-3}	4.6×10^{-3}	9.2×10^{-3}	–	–	–
Error in $L(\Omega)$†	–	–	1.3×10^{-3}	1.7×10^{-3}	3.9×10^{-3}	–	–	–
Σq	0.00	−0.01	0.030	0.031	−0.013	−0.02	−1.36	0.01

† See Flensburg & Maslen (2000) for definition.

likely reason is a small isotropic discrepancy in the unit-cell dimensions. A significant temperature dependence of the Mn—Mn bond length has been previously noted (Martin *et al.*, 1982), with the reduction at low temperatures being attributed (Martin *et al.*, 1982; Veillard & Rohmer, 1992) to the compressibility of the bond and depopulation of excited vibrational states. However, as Table 4 shows, the situation is less clear with the new data. While our value lies between those reported at 74 and 120 K, it is much closer to the latter. Moreover, the value at 296 K is *less* than that at 120 K and we conclude that there is little evidence for a significant bond lengthening between 100 and 296 K.

In all the studies the shortest Mn—C bond is Mn1—C1 and the longest C—O bond is C1—O1. These distances have been suggested as evidence (Churchill *et al.*, 1981) of greater π back-donation from the Mn atom to the axial carbonyl ligand CO(1) than to either of the mutually *trans* pairs of equatorial CO ligands. As previously observed, the $Mn(CO)_5$ fragments show small deviations from idealized square-pyramidal C_{4v} symmetry. Thus, the C—Mn—C angles for both the mutually *trans* pairs of equatorial carbonyls deviate significantly from linearity, bending towards the symmetry-related Mn1*A* center. There is an inverse relationship between the deviations from linearity of the equatorial Mn—C—O angles and the 1,3 Mn···C contact distances. Thus, the M—C—O angle which is closest to linearity, Mn1—C2—O2 178.96 (9)°, is associated with the shortest such contact Mn1*A*···C2 3.2579 (3) Å, while the least linear carbonyl Mn1—C3—O3 175.99 (3)° is associated with the longest contact Mn1*A*···C3 3.4595 (3) Å. This observation suggests that these small deviations from linearity are not due to 1,3 semi-bridging interactions, a conclusion also borne out by the topology of the electron density (see below), where no 1,3 Mn···C interactions are indicated.

3.2. Thermal motion analysis

The anisotropic displacement parameters (a.d.p.'s) obtained from a multipole refinement are, to a large extent, free from contamination from bonding density effects and thus should provide a more genuine estimation of the thermal motion of the corresponding atoms. In the best instances (Iversen *et al.*, 1996) they are very close to the neutron diffraction values. The thermal motion in (1) was analysed using the TLS formalism

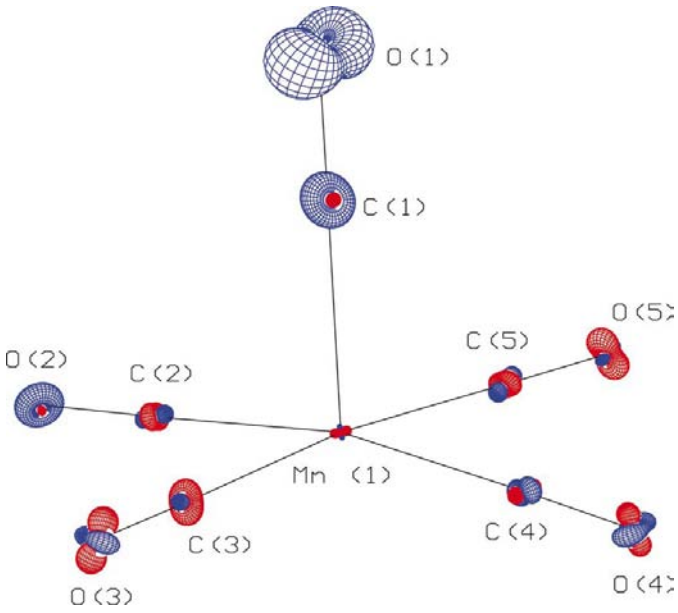

Figure 2
PEANUT (Hummel *et al.*, 1990) plot of (1) showing the RMS displacement surface of the difference a.d.p.'s (observed model) at the 99.99% probability level. Positive surfaces shown in blue, negative surfaces in red.

Table 4
Bond distances (Å) and angles (°) for (1).

Column 1: this study, taken from multipole refinement; column 2: taken from Martin *et al.* (1982); column 3: taken from Bianchi *et al.* (2000); column 4: taken from Churchill *et al.* (1981).

Temperature	100 K	74 K	120 K	296 K
Space group used for refinement	*I*2/*a*	*I*2/*a*	*C*2/*c*	*I*2/*a*
Mn1—Mn1*A*	2.9031 (2)	2.8950 (6)	2.9042 (8)	2.9038 (6)
Mn1—C1	1.8224 (4)	1.815 (2)	1.8199 (16)	1.811 (3)
Mn1—C2	1.8593 (3)	1.855 (2)	1.8537 (8)	1.850 (2)
Mn1—C3	1.8567 (3)	1.848 (2)	1.8525 (10)	1.853 (2)
Mn1—C4	1.8589 (3)	1.857 (2)	1.8524 (7)	1.854 (2)
Mn1—C5	1.8664 (3)	1.865 (2)	1.8571 (9)	1.865 (2)
C1—O1	1.1472 (6)	1.146 (3)	1.144 (4)	1.134 (4)
C2—O2	1.1420 (4)	1.139 (3)	1.1402 (12)	1.131 (3)
C3—O3	1.1437 (4)	1.142 (3)	1.1397 (15)	1.124 (3)
C4—O4	1.1433 (4)	1.134 (2)	1.1383 (11)	1.134 (4)
C5—O5	1.1420 (4)	1.139 (3)	1.1390 (13)	1.128 (3)
Mn1*A*—Mn1—C1	175.57 (1)	175.33 (6)	175.89 (7)	177.03 (9)
Mn1*A*—Mn1—C2	83.24 (1)	82.97 (4)	83.43 (4)	84.61 (7)
Mn1*A*—Mn1—C3	90.49 (1)	90.60 (4)	90.20 (4)	89.16 (7)
Mn1*A*—Mn1—C4	86.54 (1)	86.63 (4)	86.46 (4)	86.25 (7)
Mn1*A*—Mn1—C5	84.40 (1)	84.28 (4)	84.48 (4)	85.51 (7)
C2—Mn1—C4	169.53 (1)	169.36 (8)	n/a	170.67 (10)
C3—Mn1—C5	174.28 (1)	174.24 (8)	n/a	174.46 (10)
C1—Mn1—C2	93.97 (1)	94.01 (9)	94.10 (5)	93.71 (11)
C1—Mn1—C3	92.99 (1)	93.00 (10)	93.10 (5)	93.29 (12)
C1—Mn1—C4	96.36 (1)	96.50 (9)	96.13 (5)	95.50 (11)
C1—Mn1—C5	92.25 (1)	92.25 (10)	92.31 (5)	92.08 (11)
Mn1—C1—O1	178.82 (8)	178.3 (3)	178.38 (15)	179.2 (3)
Mn1—C2—O2	178.96 (9)	178.4 (2)	178.96 (14)	178.5 (2)
Mn1—C3—O3	175.99 (3)	176.17 (17)	175.91 (13)	176.3 (2)
Mn1—C4—O4	178.13 (5)	177.9 (2)	178.40 (9)	178.1 (2)
Mn1—C5—O5	178.58 (4)	178.60 (17)	178.48 (12)	178.5 (3)

(Schomaker & Trueblood, 1968). The crystallographically independent $Mn(CO)_5$ fragment was treated as a single rigid group. Table 5 gives the eigenvectors and eigenvalues of the L and T tensors in the inertial frame of reference. The rigid-body motion accounts well for the experimental a.d.p.'s (r.m.s. of $w\Delta U^{ij}$ is 4×10^{-4} Å^2, $wR = 0.065$), with both the L and T tensors being approximately isotropic. The greatest discrepancy is for the axial atoms C1 and especially O1, this extra motion being attributed to a low energy axial Mn—C—O deformation mode. Fig. 2 shows a *PEANUT* plot (Hummel *et al.*, 1990), which graphically illustrates the difference between the experimental and calculated (rigid-body) a.d.p.'s.

3.3. Atomic charges

The atomic charge polarizations which occur on chemical bonding are of fundamental interest to chemists, but unfortunately the concept of atomic charges has proved difficult to quantify accurately. In part this arises because of the problem (Wiberg & Rablen, 1993) of experimentally measuring such charges. Meister & Schwartz (1994) have conducted a principal component analysis on the charges derived from some 25 different physical and theoretical methods. They conclude that, while 'there indeed exists something in nature which corresponds to the vague charge concepts of the chemists and physicists', the scale of the derived charges can differ by a factor of ∼10, depending on the chosen method. In the past, various schemes have been adopted in charge density studies (Coppens, 1997) to partition charge to individual atomic centers, some more arbitary than others (see, for example, MRM). Within the multipole formalism (Hansen & Coppens,

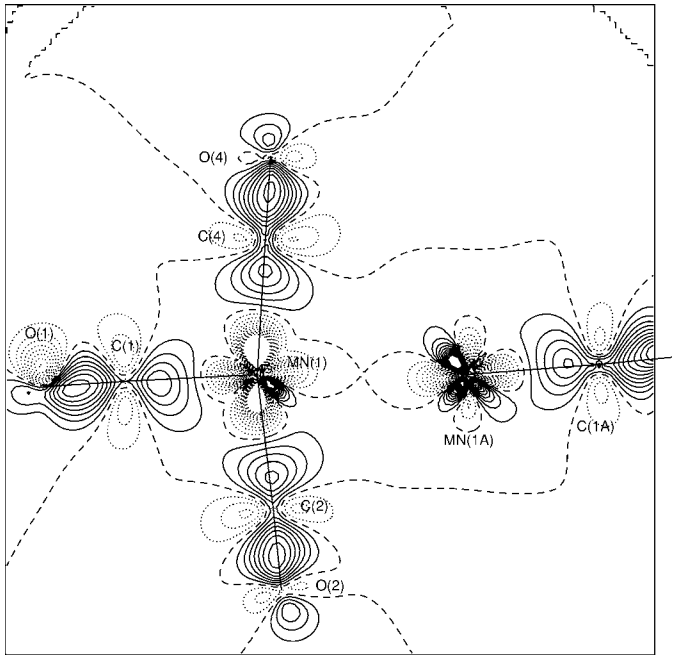

Figure 3
Static model deformation map ($\rho_{mult} - \rho_{sph}$) for (1). Positive contours are drawn as solid lines, negative contours as dotted lines and the zero contour as a dashed line. Contours are drawn at intervals of 0.1 e Å^{-3}.

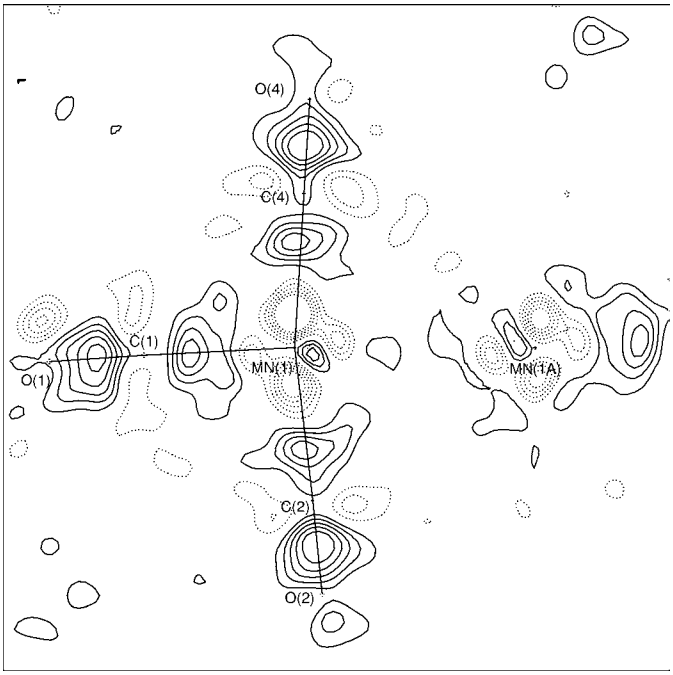

Figure 4
Experimental deformation map ($F_{obs} - F_{sph}$). Positive contours are drawn as solid lines, negative contours as dotted lines. Contours are drawn at intervals of 0.1 e Å^{-3}.

Table 5
Eigenvectors and eigenvalues from TLS analysis on (1).

L tensor	Xi(1)	Xi(2)	Xi(3)	Value (deg^2)	R.m.s. (°)
	0.89744	0.30312	−0.32049	6.61	2.57
	−0.25301	0.94884	0.18892	9.85	3.14
	0.36136	−0.08846	0.92882	4.22	2.05

T tensor				Value (Å^2)	R.m.s. (Å)
	0.96739	−0.2078	−0.14482	0.0191	0.138
	0.25168	0.85301	0.45720	0.0122	0.111
	0.02853	−0.47874	0.87749	0.0103	0.102

1978), it is usual to consider the monopole populations as defining the charge partitioning. However, the AIM approach (Bader, 1990) offers an alternative and less arbitrary method of determining atomic charges, albeit at significant computational cost. The AIM charges are obtained by numerical integration over the volume enclosed by the zero-flux surface of each atom (the atomic basin). They have been shown to be relatively insensitive to the choice of basis set (Cioslowski *et al.*, 1990), but generally lead to larger atomic charges. This is found to be the case in this study. They also have the considerable advantage that a direct comparison is possible between charges derived from the experimental and theoretical densities.

The atomic charges determined from the experimental monopole populations $q(Pv)$ and from atomic basin integrations [the AIM charges $q(\Omega)$] of both the experimental and theoretical densities, as well as those from the MRM & BGM studies, are shown in Table 3. In view of the differing partitioning schemes used in these methods, it is not surprising that there are some major disagreements. As determined by the monopole populations, the O atoms bear small positive charges and are effectively electro-neutral within experimental error, while the C atoms bear small negative charges. In contrast, the AIM method produces substantial negative charges on all O atoms and positive charges on all C atoms, which is more in keeping with their relative electro-negativities. In our study, all methods agree in assigning a substantial positive charge to the metal atom. Moreover, the AIM charges derived from the experimental and theoretical densities are in good agreement with each other, despite the fact that the calculations are based on an isolated molecule. These charges indicate the chemical bonding between the CO ligands and the metal results in an average transfer of ∼0.2 e from the metal to each carbonyl group. However, the charges depend on several factors and cannot be taken simply as an indicator of π-back donation. Experimentally, the charge transfer is greatest for CO(3) (av. −0.31 e) and least for CO(2) (av. −0.17 e), but the theoretical study implies the charge transfer is virtually identical for all CO ligands. Certainly, the AIM charges do not provide any supporting evidence for the assertion (Churchill *et al.*, 1981) that π-back donation is greatest for the axial CO(1). The calculated AIM charge in free CO is ±1.1–1.2 a.u. (MacDougall & Hall, 1990; Cioslowski *et al.*, 1990; Hernández-Trujillo & Bader, 2000), so these results indicate a small overall charge transfer to the O atoms. The AIM charges in (1) are similar to those determined for $Cr(CO)_6$ (MacDougall & Hall, 1990). The monopole charges reported by BGM are broadly similar to those obtained in this study. The major

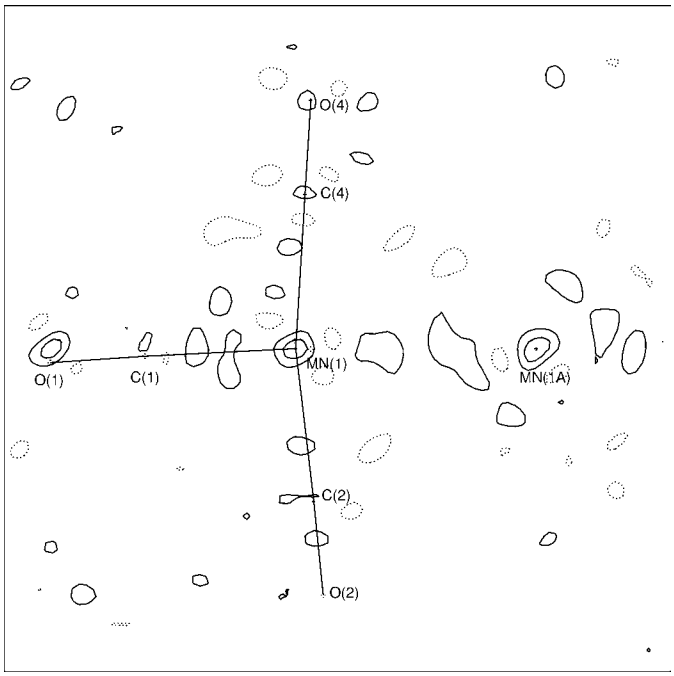

Figure 5
Final residual map ($F_{obs} - F_{mult}$) for (1). Positive contours are drawn as solid lines, negative contours as dotted lines. Contours are drawn at intervals of 0.1 e Å^{-3}.

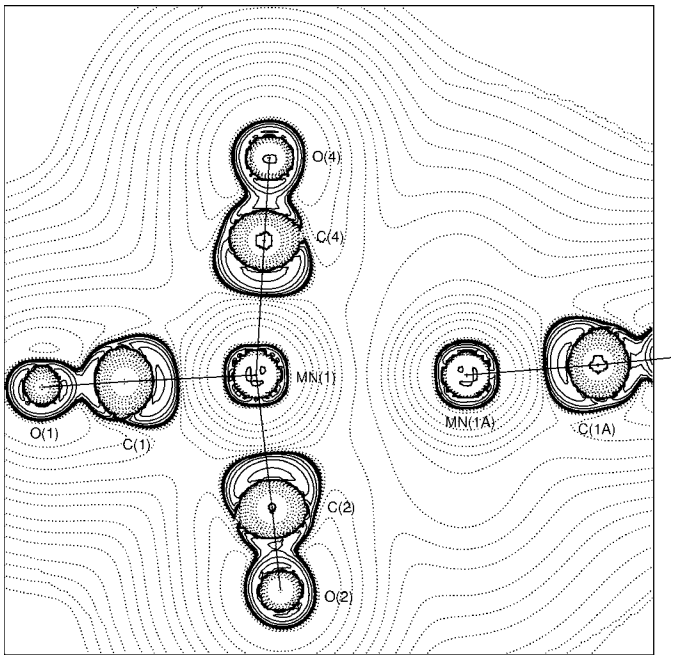

Figure 6
Laplacian function $L(\mathbf{r}) \simeq -\nabla^2\rho(\mathbf{r})$ of the experimental density. Negative contours are shown as dotted lines and indicate regions of local charge depletion. Contours are drawn at $\pm2.0 \times 10^n$, $\pm4.0 \times 10^n$, $\pm8.0 \times 10^n$ ($n = -3, -2, -1, 0, +1$) e Å^{-5}.

Table 6
Derived *d*-orbital populations (a.u.).

	This work		Holladay *et al.* (1983)	
a_1 (d_{z^2})	0.747 (21)	17.3%	0.76 (3)	14.2%
b_2 ($d_{x^2-y^2}$)	0.309 (18)	7.2%	0.65 (4)	12.1%
b_1 (d_{xy})	0.921 (18)	21.3%	1.27 (4)	23.6%
e (d_{xz})	1.168 (16)	54.2%	2.69 (3)	50.1%
d_{yz}	1.173 (18)			
Total *d* population	4.317		5.83	

difference is that the Mn atom has a small *negative* charge in BGM, although the s.u. is high.

3.4. *d*-orbital populations

As shown by Holladay *et al.* (1983) there is a direct relationship, for transition metal compounds, between the multipole populations and the *d*-orbital populations. Table 6 shows a comparison between our data and a previous analysis on $Mn_2(CO)_{10}$ (Holladay *et al.*, 1983). Simple ligand field theory leads to an expected destabilization of the e_g over the t_{2g} orbitals. This is evident from both studies, but is more marked in ours. In addition, our results show a more marked destabilization of b_2 *versus* a_1 than the previous work, and a significantly lower overall *d*-orbital population. Nevertheless, the percentage ratios t_{2g}/e_g agree reasonably well. Abramov *et al.* (1998) have undertaken a similar analysis on the closely related molecule $HMn(CO)_4(PPh_3)$ and find a t_{2g}:e_g population ratio of 71.5:28.5. The significantly non-zero populations of the e_g set is consistent with covalency in the Mn—C bonds.

3.5. Deformation maps

The static model deformation map in the plane containing C1—C2—C4 is shown in Fig. 3. The plot for the corresponding plane C1—C3—C5 is similar. As expected, there is significant charge accumulation into the C—O and Mn—C bonds and charge depletion at the Mn center. The midpoint of the Mn–Mn vector corresponds to an area of zero depletion, indicating that at this point there is no charge redistribution relative to the spherical atom model. These features are well reproduced in the experimental deformation map, Fig. 4, and the final residual maps (see Fig. 5) show no significant features, with the largest peak of 0.274 e Å^{-3} close to the Mn centre. As is more clearly demonstrated in the topological analysis, there is no significant charge accumulation at the centre of the Mn–Mn vector, a result which is in good agreement with the previous studies of Martin *et al.* (1982) and Bianchi *et al.* (2000). The small sharp feature next to the Mn atom may indicate some minor uncorrected systematic error in the data.

3.6. Topological analysis of electron density

Table 2 lists important topological properties obtained from this study, compared with those from BGM. Apart from a significant difference elaborated below, the agreement between the two studies is reasonable. The expected (3,−1) bond critical points (b.c.p.) were found between all covalently bonded atoms. According to Bader (1998), this provides a universal indicator of bonding between these atoms. No critical points corresponding to 1,3 Mn···C interactions between the Mn atom and the carbonyl ligands on the symmetry-related Mn1*A* atom were detected. However, in a study on $M(\mu$-CO$)M$ systems, Macchi & Sironi (2003) conclude that although no bond path is observed where the 1,3 $M\cdots$C interaction is weak, these interactions may provide non-negligible components to bonding, and contribute to the small $M-M$ bond orders which are often observed.

Numerous high-level theoretical studies on (1) have been reported, including AIM analyses on the SCF density (Bo *et al.*, 1993; MacDougall, 1989) as well as recent DFT studies by Rosa *et al.* (1995) and Folga & Ziegler (1993). Since neither of these DFT studies reported an AIM analysis, we have undertaken a DFT study of (1) at the 6-311+G* B3LYP level to provide a reference density. These theoretical results are reported in Table 2. Not withstanding the fact that our theoretical calculations are based on an isolated gas-phase molecule, there is a very reasonable agreement between the topological properties of the experimental and theoretical densities. Volkov, Abramov & Coppens (2000) have recently demonstrated that the effect of the crystal lattice on intramolecular topological properties is surprisingly small. A map of the Laplacian function $L(\mathbf{r}) \simeq -\nabla^2\rho(\mathbf{r})$ of the experimental density through the same molecular plane as previous figures is given in Fig. 6, and that of the theoretical density in the region of the Mn—Mn bond from different basis sets in Fig. 7.

Both our own and the BGM experimental studies give similar values for the density $\rho(\mathbf{r}_b)$ and small *positive* values for the Laplacian of the density $\nabla^2\rho(\mathbf{r}_b)$ at the b.c.p. between the two Mn centers. In contrast, the theoretical AIM studies of MacDougall (1989) and Bo *et al.* (1993), while giving similar values of $\rho(\mathbf{r}_b)$ (0.209 and 0.202 e Å^{-3} respectively), showed *negative* values for $\nabla^2\rho(\mathbf{r}_b)$ (−0.144 and −0.241 e Å^{-5}, respectively). A flat region of negative Laplacian at the midpoint of the Mn centers is reproduced in our theoretical study when using a relatively limited basis set, see Fig. 7(*b*). This island has been attributed (MacDougall, 1989) to the remains of the fourth shell of charge concentration of both Mn atoms. However, as previously alluded by Macchi *et al.* (1998*b*) and confirmed by our own calculations, the sign of $\nabla^2\rho(\mathbf{r}_b)$ for the Mn—Mn bond is strongly dependent on the basis set employed. As Fig. 7(*a*) shows, when an extensive basis with diffuse functions on the Mn atoms is used, no such island is observed and we therefore conclude it is an artefact. It should be emphasized that although this feature is obvious in the Laplacian functions shown in Fig. 7, the actual difference in electron density is minimal. At the mid-point of the Mn—Mn bond, the difference in the densities derived from the two basis sets is less than 10^{-3} e Å^{-3}.

According to Bader (1990) and Cremer & Kraka (1984*a*,*b*), atomic interactions may be characterized according to the values of $\rho(\mathbf{r}_b)$ and $\nabla^2\rho(\mathbf{r}_b)$ and also the kinetic energy density $G(\mathbf{r}_b)$ and the local energy density $H(\mathbf{r}_b)$ [*i.e.* $G(\mathbf{r}_b) + V(\mathbf{r}_b)$] at the (3,−1) bond critical points in electron density. Shared or open-shell (covalent) interactions, where the potential energy density $V(\mathbf{r}_b)$ dominates over the kinetic energy density in the

Table 7
Integrated densities over interatomic surfaces of (1).

Bond	Density ρ (e Å^{-1})	Surface area (Å^2)
Mn1—Mn1*A*	1.819	37.245
Mn1—C1	2.177	16.503
Mn1—C2	2.316	22.655
Mn1—C3	2.244	20.662
Mn1—C4	2.299	21.861
Mn1—C5	2.298	21.738
C1—O1	3.176	10.891
C2—O2	3.302	14.778
C3—O3	3.249	13.284
C4—O4	3.280	14.296
C5—O5	3.296	14.666

region of the interatomic surface, are characterized by large values of $\rho(\mathbf{r}_b)$ and negative values of $\nabla^2\rho(\mathbf{r}_b)$ and $H(\mathbf{r}_b)$. Closed-shell (ionic) interactions, where the kinetic energy density $G(\mathbf{r}_b)$ dominates over the potential energy density in the region of the interatomic surface, are characterized by small values of $\rho(\mathbf{r}_b)$, positive values of $\nabla^2\rho(\mathbf{r}_b)$ and positive, near-zero values of $H(\mathbf{r}_b)$. As we (Smith *et al.*, 1997) and others (Macchi *et al.*, 1998*a*,*b*, 1999; Koritsansky & Coppens, 2001; Macchi & Sironi, 2003) have previously noted, the topological properties of covalent bonds involving transition metals do not have the same characteristics as covalent bonds between first-row atoms.

The small values of $\rho(\mathbf{r}_b)$ and $\nabla^2\rho(\mathbf{r}_b)$ for the Mn—Mn bond are typical of those found in other theoretical and experimental studies on transition metal compounds containing metal–metal bonds (see, for example, Macchi *et al.*, 1998*b*, 1999; Bo *et al.*, 1990, 1993; Macchi & Sironi, 2003). These low values do not necessarily indicate weak chemical bonds. The integrated density over the whole zero-flux surface linking two atoms may provide a better indicator of their bond strength (Cremer & Kraka, 1984*a*). The integrated densities (from the theoretical study) over the interatomic surfaces for all unique bonds in (1) are given in Table 7. The integrated density in the Mn—Mn bond is substantial and quite similar in value to those for the Mn—C bonds and moreover is in agreement with values quoted by Macchi & Sironi (2003) for related compounds. The total energy density is negative, albeit marginally so, while for closed-shell 'ionic' interactions it is invariably positive (Cremer & Kraka, 1984*a*). For these reasons, we prefer to categorize the Mn—Mn bonding in (1) as open-shell and covalent, rather than metallic and 'between ionic and covalent', as described by BGM.

In both the experimental studies the Mn—C bonds show very similar values of $\rho(\mathbf{r}_b)$ and $\nabla^2\rho(\mathbf{r}_b)$, which are in good agreement with the theoretical values. The positive values of $\nabla^2\rho(\mathbf{r}_b)$ found here concur with numerous theoretical and experimental studies on transition metal complexes, which almost invariably show a positive Laplacian for any bonds involving the transition metal. These positive values should not be taken to indicate a closed-shell (ionic) interaction between the Mn and C atoms. The very high density at the heavier atoms results in the λ_3 curvature being large and positive and thus dominating the value of $\nabla^2\rho(\mathbf{r}_b)$. Furthermore, Macchi *et al.* (1998*b*) have argued convincingly, on the basis of the topology of $\nabla^2\rho$ along the bond path, that the metal–metal and metal–ligand bonds in $Co_2(CO)_6(AsPh_3)_2$

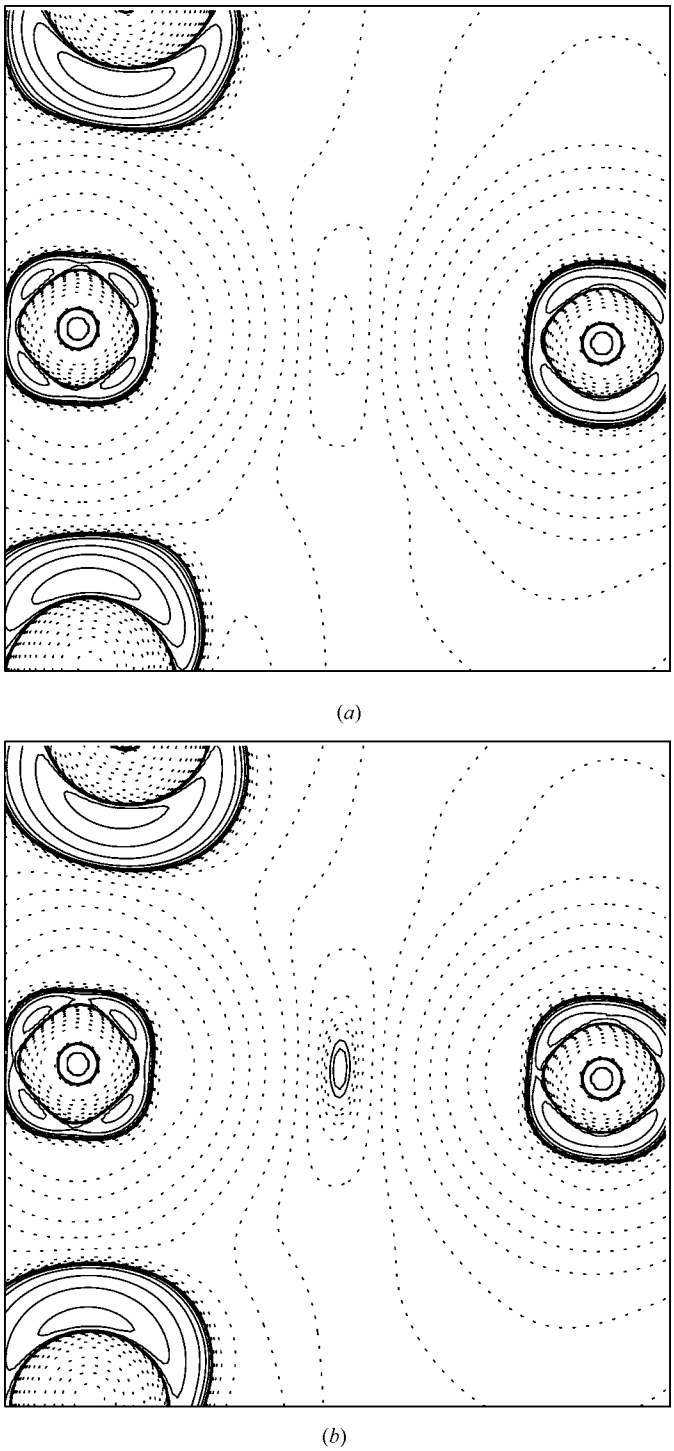

(*a*)

(*b*)

Figure 7
Laplacian function $L(\mathbf{r}) \equiv -\nabla^2\rho(\mathbf{r})$ of the DFT theoretical density (*a*) from BASIS 3 set calculation including diffuse functions; (*b*) from minimal BASIS 1 set (see text) in the region of the Mn—Mn bond. Negative contours are shown as dotted lines and indicate regions of local charge depletion. Contours are drawn at $\pm2.0 \times 10^n$, $\pm4.0 \times 10^n$, $\pm8.0 \times 10^n$ (n = −3,−2,−1,0,+1) e Å^{-5}.

Table 8
Properties of critical points in $-\nabla^2\rho(\mathbf{r})$ in the *i*-VSCC of (1).

Experimental values in parentheses.

	Rho (e Å^{-3})	$-\nabla^2\rho(\mathbf{r})$ (e Å^{-5})	Distance from nucleus (Å)
(3,−3) critical points	20.20 (19.10)	−855.32 (−720.25)	0.339 (0.339)
	20.14 (20.11)	−846.47 (−779.66)	0.338 (0.337)
	20.27 (19.37)	−864.26 (−708.45)	0.338 (0.339)
	20.06 (19.59)	−836.78 (−746.01)	0.339 (0.338)
	20.16 (20.24)	−848.31 (−789.88)	0.338 (0.337)
	20.26 (19.89)	−862.28 (−814.24)	0.339 (0.336)
	20.11 (19.65)	−843.55 (−763.98)	0.338 (0.337)
	20.27 (19.55)	−864.28 (−728.70)	0.338 (0.338)
(3,−1) critical points	18.85 (18.25)	−683.79 (−610.32)	0.343 (0.341)
	18.92 (18.79)	−674.50 (−623.44)	0.344 (0.341)
	18.83 (17.93)	−680.66 (−541.07)	0.343 (0.344)
	18.86 (n/a)	−664.01 (−666.73)	0.344 (0.339)
	18.98 (18.15)	−682.34 (−568.71)	0.343 (0.343)
	18.87 (19.18)	−668.23 (−659.54)	0.343 (0.340)
	18.95 (19.27)	−678.78 (−663.54)	0.343 (0.340)
	18.82 (18.60)	−679.52 (−649.56)	0.343 (0.340)
	18.92 (19.30)	−674.78 (−643.11)	0.343 (0.340)
	18.90 (18.57)	−670.94 (−586.01)	0.344 (0.342)
	18.85 (18.37)	−666.39 (−578.33)	0.344 (0.342)
	18.84 (18.56)	−681.52 (−625.25)	0.343 (0.341)
(3,+1) critical points	14.91 (15.84)	−189.91 (−240.42)	0.360 (0.352)
	14.87 (14.15)	−187.09 (−126.52)	0.361 (0.360)
	15.21 (17.63)	−197.40 (−337.24)	0.360 (0.349)
	15.52 (17.11)	−234.83 (−314.67)	0.359 (0.350)
	14.84 (16.15)	−183.68 (−254.94)	0.361 (0.351)
	14.94 (14.81)	−193.03 (−172.66)	0.360 (0.356)

should be considered as genuine covalent interactions, a result which has general implications. This view is, of course, consistent with chemical common sense.

The major area of disagreement between our study and BGM lies in the topology of the C—O bonds, and this is a well recognized issue (Macchi & Sironi, 2003). The b.c.p. in CO lies very close to the nodal plane in $\nabla^2\rho$ and the CO bond is classified by Bader (1990) as an *intermediate* interaction. Depending on the level and quality of *ab initio* calculation (Bader, 1990; Aray & Rodríguez, 1996), the values of $\rho(\mathbf{r}_b)$ and $\nabla^2\rho(\mathbf{r}_b)$ for free CO fall in the ranges 3.31–3.44 e Å^{-3} and 6.48–23.6 e Å^{-5}, respectively. In metal carbonyl complexes, it has been long recognized (MacDougall & Hall, 1990) that the Laplacian of coordinated CO closely resembles that of the free ligand and a similar situation arises regarding the position of the b.c.p. Our experimental values of $\nabla^2\rho(\mathbf{r}_b)$ for (1) are very close to the theoretical values, but differ significantly from those of BGM, in sign as well as magnitude. Moreover, the position of the b.c.p. relative to the nodal plane, and hence the magnitude of $\nabla^2\rho(\mathbf{r}_b)$, is crucially dependent on the deformation valence radial scaling parameters κ' for the O and C atoms. In other experimental studies, both positive (*e.g.* Abramov *et al.*, 1998) and negative values (*e.g.* Macchi*et al.*, 1998*b*) have been found for $\nabla^2\rho(\mathbf{r}_b)$ in CO bonds and this parameter must be regarded as rather unreliable.

From Table 2, it can be seen that the approximation of Abramov (1997) for $G(\mathbf{r}_b)$ is excellent for the Mn—Mn and Mn—C bonds, and quite reasonable for the C—O bonds. The $R_{\rm para}$ value (see Table 2 for definition) allows a quantitative comparison of the quality of fit between the experimental and theoretical properties. These show that, as expected, the most extensive basis (BASIS 3) gives the best fit to the majority of the experimentally derived properties. Surprisingly, the minimal basis BASIS 1 provides the best fit to the individual eigenvalues of the Hessian $\lambda_{1,2,3}$, although not to the magnitude of $\nabla^2\rho(\mathbf{r}_b)$. For all bonds, there is excellent agreement regarding $\rho(\mathbf{r}_b)$ and a respectable agreement with $\nabla^2\rho(\mathbf{r}_b)$. The worst discrepancies occur for the ellipticity parameter ε, but in virtually all cases $R_{\rm param}$ is significantly smaller with our experimental results than with those of BGM.

3.7. Topological analysis of the Laplacian of the electron density

The experimental Laplacian map, $L(\mathbf{r}) \equiv -\nabla^2\rho(\mathbf{r})$, in the C1—C2—C4 plane is shown in Fig. 6 and theoretical maps in the same plane in Fig. 7. While there are striking similarities between the two maps, there are two small features of divergence, *viz*:

(i) the above-mentioned presence of a small rise in $L(\mathbf{r})$ in the theoretical maps at the center of the Mn—Mn bond;

(ii) the torus of charge depletion at the C atoms, normally observed for CO ligands (Aray & Rodríguez, 1996), is more prominent in the theoretical maps.

As expected for a first-row transition metal (Bader & Matta, 2001), the Mn atom shows only three shells of charge

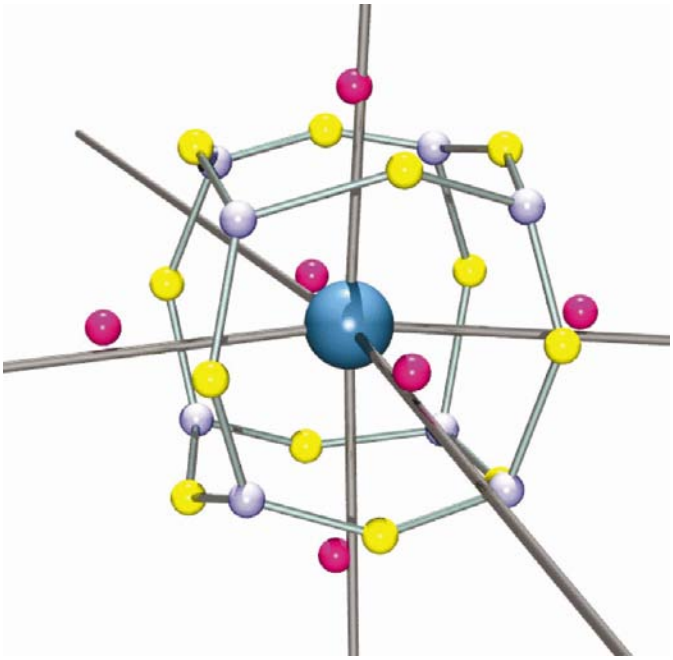

Figure 8
The atomic graph of the Mn atom, taken from the experimental study. The pink spheres represent the (3,+1) critical points of charge depletion, the light blue spheres the (3,−3) critical points of charge concentration and the yellow spheres the saddle (3,−1) critical points in $L(\mathbf{r}) \simeq -\nabla^2\rho(\mathbf{r})$ The atom C5 is towards the viewer, Mn1*a* vertically downwards and atom C2 to the right.

concentrations in $L(\mathbf{r})$. The 3*d* electrons are subsumed with the core 3*s* and 3*p* into the *inner* valence shell charge concentration (*i*-VSCC), which is distinctly non-spherical (Gillespie *et al.*, 1996). A topological analysis of $L(\mathbf{r})$ in the region of the *i*-VSCC was undertaken, on both the theoretical and experimental density. The results, reported in Table 8, are in reasonable agreement, especially for the (3,−3) and (3,−1) critical points. These points, in the region of ∼0.33–0.36 Å from the nucleus, constitute the atomic graph (Bader, 1990) of the Mn atom, shown in Fig. 8. The graph has the topology of a cube and is consistent with the octahedral coordination, with the *d*-orbital populations and with the qualitative expectations of ligand field theory, in that the core-like 3*d* electrons avoid the charge concentrations of the carbonyl ligands. There are six (3,+1) critical points of charge depletion in the direction of the octahedral axes (in the face of the cube), eight (3,−3) critical points of non-bonded charge concentration in the center of each face of the octahedron (in the corners of the cube) and 12 (3,−1) critical points along all the edges of the cube. Slightly outside the VSCC in the region of Valence Shell Charge Depletion (VSCD), around 0.51 Å from the nucleus, six (3,+3) critical points of charge depletion are found lying on the six bond paths emanating from the manganese atom. An essentially identical atomic graph was obtained by Abramov *et al.* (1998) for the closely related molecule $HMn(CO)_4(PPh_3)$ in an experimental study. This result supports our view that the chemical environments of the Mn atoms in (1) and $HMn(CO)_4(PPh_3)$, in so far as they are manifest in the atomic graph of that atom, are closely similar. This result provides further confirmation of the covalent nature of the Mn—Mn bond. Theoretical studies on $L(\mathbf{r})$ in the region of the *i*-VSCC of the octahedrally coordinated metal atoms in $Fe_2(CO)_9$ (Bo *et al.*, 1993) and $Cr(CO)_6$ (MacDougall & Hall, 1990) also show identical atomic graphs to those described above. In contrast, BGM report only six (3,−3) critical points of non-bonded charge concentration in their study on (1).

4. Conclusions

On a qualitative level, there is good agreement between the topology of the electron densities observed in our study and that of BGM. The same set of critical points, with broadly similar values of $\rho(\mathbf{r}_b)$, were obtained. Judging from the lower residuals and s.u.'s on derived metric parameters, and the greater internal consistency in the derived multipole parameters, the quality of the data obtained using a CCD detector appears superior to that of the BGM study. Despite some qualitative differences, particularly in the Laplacian values $\nabla^2\rho(\mathbf{r}_b)$ in CO bonds, the level of agreement between the two studies is encouraging. Moreover, and notwithstanding the fact that our theoretical calculations are based on an isolated gas-phase molecule, there is excellent agreement between the topological properties of our experimental and theoretical densities. The function proposed by Abramov (1997) for $G(\mathbf{r})$ at the b.c.p. is shown to give an excellent approximation to values derived from theory. Previous conclusions about the bonding in molecule (1) have been confirmed, particularly the lack of evidence for 1,3 Mn···C interactions. We prefer a description of the bonding in (1) in terms of covalent interactions, rather than the 'closed-shell' description given by BGM.

We thank the EPSRC for grant GR/M91433 towards the purchase of a KappaCCD diffractometer and for access to the Columbus DEC 8400 Superscalar Service (RAL). We especially thank Professors Piero Macchi (Milano) and Anatoliy Volkov (Buffalo) for many helpful discussions and advice on the XD and TOPXD programs.

References

Abramov, Y. A. (1997). *Acta Cryst.* A**53**, 264–272.
Abramov, Y. A., Brammer, L., Klooster, W. T. & Bullock, R. M. (1998). *Inorg. Chem.* **37**, 6317–6328.
Aicken, F. M. & Popelier, P. L. A. (2000). *Can. J. Chem.* **78**, 415–426.
Aray, Y. & Rodríguez, J. (1996). *Can. J. Chem.* **74**, 1014–1020.
Bader, R. F. W. (1990). *Atoms in Molecules: A Quantum Theory.* Oxford: Clarendon Press.
Bader, R. F. W. (1998). *J. Phys. Chem. A*, **102**, 7314–7323.
Bader, R. F. W. & Matta, C. F. (2001). *Inorg. Chem.* **40**, 5603–5611.
Bauschlicher, Jr, C. W., Langhoff, S. R. & Barnes, L. A. (1989). *J. Chem. Phys.* **91**, 2399–2411.
Becke, A. D. (1993). *J. Chem. Phys.* **98**, 5648–5652.
Becker, P. J. & Coppens, P. (1974). *Acta Cryst.* A**30**, 129–147.
Bianchi, R., Gervasio, G. & Marabello, D. (2000). *Inorg. Chem.* **39**, 2360–2366.
Bianchi, R., Gervasio, G. & Marabello, D. (2001*a*). *Helv. Chim. Acta*, **84**, 722–734.
Bianchi, R., Gervasio, G. & Marabello, D. (2001*b*). *Acta Cryst.* B**57**, 638–645.
Biegler-König, F. (2000). *J. Comput. Chem.* **12**, 1040–1048.
Biegler-König, F. W., Bader, R. F. W. & Tang, T.-H. (1982). *J. Comput. Chem.* **3**, 317–328.
Blessing, R. H. (1995). *Acta Cryst.* A**51**, 33–38.
Blessing, R. H. (1997*a*). *DENZOX*. Modified for KappaCCD data by L. J. Farrugia & K. W. Muir (2001). University of Glasgow.
Blessing, R. H. (1997*b*). *J. Appl. Cryst.* **30**, 421–426.
Bo, C., Poblet, J.-M. & Bénard, M. (1990). *Chem. Phys. Lett.* **169**, 89–96.
Bo, C., Sarasa, J.-P. & Poblet, J.-M. (1993). *J. Phys. Chem.* **97**, 6362–6366.
Brown, D. A., Chambers, W. J., Fitzpatrick, A. J. & Rawlinson, S. R. M. (1971). *J. Chem. Soc. A*, pp. 720–725.
Bunge, C. F., Barrientos, J. A. & Bunge, A. V. (1993). *At. Data Nucl. Data Tab.* **53**, 113–162.
Bürgi, H. B. (1984). *Trans. Am. Cryst. Assoc.* **20**, 61–71.
Bytheway, I., Figgis, B. N. & Sobolev, A. N. (2001). *J. Chem. Soc. Dalton Trans.* pp. 3285–3294.
Bytheway, I., Grimwood, D. J. & Jayatilaka, D. (2002). *Acta Cryst.* A**58**, 232–243.
Churchill, M. R., Amoh, K. N. & Wasserman, H. J. (1981). *Inorg. Chem.* **20**, 1609–1611.
Cioslowski, J., Hay, P. J. & Ritchie, J. P. (1990). *J. Phys. Chem.* **94**, 148–151.
Coppens, P. (1984). *Acta Cryst.* A**40**, 184–195.
Coppens, P. (1985). *Coord. Chem. Rev.* **65**, 285–307.
Coppens, P. (1997). *X-ray Charge Densities and Chemical Bonding.* Oxford: Oxford Science Publications.
Coppens, P. (1998). *Acta Cryst.* A**54**, 779–788.
Cremer, D. & Kraka, E. (1984*a*). *Croat. Chem. Acta*, **57**, 1259–1281.
Cremer, D. & Kraka, E. (1984*b*). *Angew Chem. Int. Ed. Engl.* **23**, 627–628.

Farrugia, L. J. (1997). *J. Appl. Cryst.* **30**, 565.
Farrugia, L. J. (1999). *J. Appl. Cryst.* **32**, 837–838.
Farrugia, L. J. & Mallinson, P. R. (2002). Unpublished observations.
Figgis, B. N., Iversen, B. B., Larsen, F. K. & Reynolds, P. A. (1993). *Acta Cryst.* B**49**, 794–806.
Flensburg, C. & Madsen, D. (2000). *Acta Cryst.* A**56**, 24–28.
Folga, E. & Ziegler, T. (1993). *J. Am. Chem. Soc.* **115**, 5169–5176.
Freund, H.-J. & Hohneicher, G. (1979). *Theor. Chim. Acta (Berlin)*, **51**, 145–162.
Freund, H.-J., Dick, G. & Hohneicher, G. (1980). *Theor. Chim. Acta (Berlin)*, **57**, 181–207.
Gillespie, R. J., Bytheway, I., Tang, T.-H. & Bader, R. F. W. (1996). *Inorg. Chem.* **35**, 3954–3963.
Graafsma, H., Svensson, S. O. & Kvick, Å. (1997) *J. Appl. Cryst.* **30**, 957–962.
Guest, M. F., Kendrick, J., van Lenthe, J. H. & Sherwood, P. (2002). *GAMMES-UK*, Version 6.3. The DFT module within GAMESS-UK was developed by Dr P. Young under the auspices of EPSRC's Collaborative Comutational Project No. 1 (CCP1, 1995–1997).
Hansen, N. K. & Coppens, P. (1978). *Acta Cryst.* A**34**, 909–921.
Herbstein, F. H. (2000). *Acta Cryst.* B**56**, 547–557.
Hernández-Trujillo, J. & Bader, R. F. W. (2000). *J. Phys. Chem.* **104**, 1779–1794.
Hirshfeld, F. L. (1976). *Acta Cryst.* A**32**, 239–244.
Holladay, A., Leung, P. & Coppens P. (1983). *Acta Cryst.* A**39**, 377–387.
Hummel, W., Hauser, J. & Bürgi, H.-B. (1990) *J. Mol. Graphics*, **8**, 214–220.
Iversen, B. B., Larsen, F. K., Figgis, B. N. & Reynolds, P. A. (1997). *J. Chem. Soc. Dalton Trans.* pp. 2227–2240.
Iversen, B. B., Larsen, F. K., Figgis, B. N., Reynolds, P. A. & Schultz, A. J. (1996). *Acta Cryst.* B**52**, 923–931.
Kirschbaum, K., Martin, A. & Pinkerton, A. A. (1997). *J. Appl. Cryst.* **30**, 514–516.
Koritsanszky, T. S. & Coppens, P. (2001). *Chem. Rev.* **101**, 1583–1627.
Koritsanszky, T., Howard, S. T., Su, Z., Mallinson, P. R., Richter, T. & Hansen, N. K. (1997) *XD*. Berlin: Free University of Berlin.
Krijn, M. P. C. M., Graafsma, H. & Feil, D. (1988). *Acta Cryst.* B**44**, 609–616.
Krug, P. & Bader, R. F. W. (1990). *AIMPAC*. Department Chemistry, McMaster University, Hamilton, Ontario, Canada.
Kuntzinger, S., Dahaoui, S., Ghermani, N. D., Lecomte, C. & Howard, J. A. K. (1999). *Acta Cryst.* B**55**, 867–881.
Leung, P. C. W. & Coppens, P. (1983). *Acta Cryst.* B**39**, 535–542.
Low, A. A., Kunze, K. L., MacDougall, P. J. & Hall, M. B. (1991). *Inorg. Chem.* **30**, 1079–1086.
Macchi, P., Garlaschelli, L., Martinego, S. & Sironi, A. (1999). *J. Am. Chem. Soc.* **121**, 10428–10429.
Macchi, P., Proserpio, D. M. & Sironi, A. (1998*a*). *J. Am. Chem. Soc.* **120**, 1447–1455.
Macchi, P., Proserpio, D. M. & Sironi, A. (1998*b*). *J. Am. Chem. Soc.* **120**, 13429–13435.
Macchi, P., Proserpio, D. M., Sironi, A., Soave, R. & Destro, R. (1998). *J. Appl. Cryst.* **31**, 583–588.
Macchi, P., Schultz, A. J., Larsen, F. K. & Iversen, B. B. (2001). *J. Phys. Chem.* **105**, 9231–9242.
Macchi, P. & Sironi, A. (2003). *Coord Chem. Rev*. In the press.
MacDougall, P. J. (1989). PhD Thesis. McMaster University, Ontario, Canada.
MacDougall, P. J. & Hall, M. B. (1990). *Trans. Am. Cryst. Assoc.* **26**, 105–123.
Martin, A. & Pinkerton, A. A. (1998). *Acta Cryst.* B**54**, 471–477.
Martin, M., Rees, B. & Mitschler, A. (1982). *Acta Cryst.* B**38**, 6–15.
Meister, J. & Schwartz, W. H. E. (1994). *J. Phys. Chem.* **98**, 8245–8252.
Nonius (1998). *Collect, DENZO(SMN), SCALEPACK, KappaCCD Program Package.* Nonius BV, Delft, The Netherlands.
Otwinowski, Z. & Minor, W. (1997). *Methods in Enzymology*, Vol. 276, *Macromolecular Crystallography*, edited by C. W. Carter Jr & R. M. Sweet, Part A, pp. 307–326. New York: Academic Press.
Paciorek, W. A., Meyer, M. & Chapuis, G. (1999). *Acta Cryst.* A**55**, 543–557.
Pérès, N., Boukhris, A., Souhassou, M., Gavoille, G. & Lecomte, C. (1999). *Acta Cryst.* A**55**, 1038–1048.
Popelier, P. L. A. (1998). *MORPHY*98. Department of Chemistry, UMIST.
Popelier, P. L. A. (2000). *Atoms in Molecules: An Introduction.* Harlow: Prentice Hall.
Powell, H. M. & Ewens, R. V. G. (1939). *J. Chem. Soc.* pp. 286–292.
Rosa, A., Ricciardi, G., Baerends, E. J. & Stufkens, D. J. (1995). *Inorg. Chem.* **34**, 3425–3432.
Schafer, A., Horn, H. & Ahlrichs, R. (1992). *J. Chem. Phys.* **97**, 2571–2577.
Scherer, W., Hieringer, W., Spiegler, M., Sirsch, P., McGrady, G. S., Downs, A. J., Haaland, A. & Pederson, B. (1998). *J. Chem. Soc. Chem. Commun.* pp. 2471–2472.
Schomaker, V. & Trueblood, K. N. (1968). *Acta Cryst.* B**24**, 63–76.
Sheldrick, G. M. (1997). *SHELXL*97. University of Göttingen, Germany.
Smith, G. T., Mallinson, P. R., Frampton, C. S., Farrugia, L. J., Peacock, R. D. & Howard, J. A. K. (1997). *J. Am. Chem. Soc.* **119**, 5028–5034.
Su, Z. & Coppens, P. (1998). *Acta Cryst.* A**54**, 646–652.
Tsirelson, V. G. & Ozerov, R. P. (1996). *Electron Density and Bonding in Crystals.* Bristol: Institute of Physics Publishing.
Veillard, A. & Rohmer, M.-M. (1992). *Int. J. Quantum Chem.* **42**, 965–976.
Volkov, A., Abramov, Yu. A. & Coppens, P. (2001). *Acta Cryst.* A**57**, 272–282.
Volkov, A., Abramov, Yu., Coppens, P. & Gatti, C. (2000). *Acta Cryst.* A**56**, 332–339.
Volkov, A. & Coppens, P. (2001). *Acta Cryst.* A**57**, 395–405.
Volkov, A., Gatti, C., Abramov, Yu. & Coppens, P. (2000). *Acta Cryst.* A**56**, 252–258.
Wachters, A. J. H. (1969). IBM Tech. Rept. RJ584.
Wachters, A. J. H. (1970). *J. Chem. Phys.* **52**, 1033–1036.
Wiberg, K. B. & Rablen, P. R. (1993). *J. Comput. Chem.* **14**, 1504–1518.
Zobel, D., Luger, P., Dreissig, W. & Koritsanszky, T. (1992). *Acta Cryst.* B**48**, 837–848.

Acta Crystallographica Section B
Structural Science
ISSN 0108-7681

addenda and errata

Experimental charge density in the transition metal complex $Mn_2(CO)_{10}$: a comparative study. Erratum

Louis J. Farrugia,[a]* Paul R. Mallinson[a] and Brian Stewart[b]

[a]Department of Chemistry, University of Glasgow, Glasgow G12 8QQ, Scotland, and [b]Department of Chemisty and Chemical Engineering, University of Paisley, Paisley PA1 2BE, Scotland. Correspondence e-mail: louis@chem.gla.ac.uk

A value is missing in the third row of the O3—C3 section of Table 3 on p. 238 of Farrugia *et al.* (2003). The missing value which should be in the fifth column is 13.757, and the remaining entries should be transfered to the next column along.

References

Farrugia, L. J., Mallinson, P. R. & Stewart, B. (2003). *Acta Cryst.* B**59**, 234–247.

